ACS APPLIED MATERIALS & INTERFACES

Research Article

www.acsami.org

Effect of B Site Coordination Environment in the ORR Activity in Disordered Brownmillerites $Ba_2In_{2-x}Ce_xO_{5+\delta}$

Chamundi P. Jijil,[†,§] Siddheshwar N. Bhange,[‡,§] Sreekumar Kurungot,*[,§,‡] and R. Nandini Devi*[,§,†]

[†]Catalysis and Inorganic Chemistry Division, CSIR-National Chemical Laboratory, Pune, India

[‡]Physical Chemistry Division, CSIR-National Chemical Laboratory, Pune, India

[§]Academy of Scientific and Innovative Research, New Delhi, India

Supporting Information

ABSTRACT: $Ba_2In_2O_5$ brownmillerites in which the In site is progressively doped with Ce exhibit excellent oxygen reduction activity under alkaline conditions. Ce doping leads to structural changes advantageous for the reaction. Twenty-five percent doping retains the ordered structure of brownmillerite with alternate layers of tetrahedra and octahedra, whereas further increase in Ce concentration creates disorder. Structures with disordered oxygen atoms/vacancies are found to be better oxygen reduction reaction catalysts probably aided by isotropic ionic conduction, and $Ba_2In_{0.5}Ce_{1.5}O_{5+\delta}$ is the most active. This enhanced activity is correlated to the more symmetric Ce site coordination environment in this compound. Stoichiometric perovskite $BaCeO_3$ with the highest concentration of Ce shows very poor activity emphasizing the importance of oxygen vacancies, which facilitate O_2 adsorption, in tandem with catalytic sites in oxygen reduction reactions.

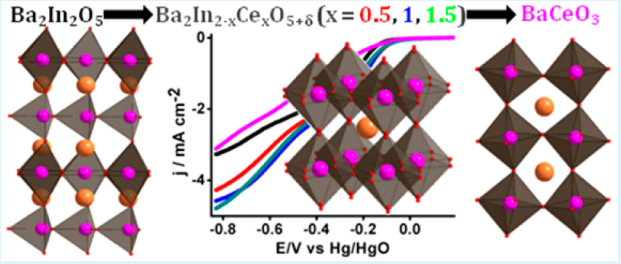

KEYWORDS: *fuel cell, oxygen reduction reaction, brownmillerite, Rietveld refinement, oxygen disorder*

1. INTRODUCTION

Sluggish kinetics of oxygen reduction reaction (ORR) in the cathode side and the consequent necessity for high concentrations of Pt in the catalyst is the primary bottleneck for extensive utilization of fuel cells in small domestic or automobile applications.[1−3] Hence, there is an urgent need to limit the usage of Pt and promote low cost, non-Pt catalysts with comparable catalytic properties.[4,5] So far, a large variety of materials have been explored as possible electrocatalysts for ORR and nitrogen doped carbon nanostructures, N4-macrocycles, oxides such as perovskites, brownmillerites, pyrochlores, and so on have been proposed to be alternative ORR catalysts.[6−14] Recent progress in the electrocatalyst development for fuel cells has revealed that stable structured oxides can open up many new avenues, especially in alkaline fuel cells. The characteristic features that make these classes of materials as ideal candidates for electrochemical applications are mixed ionic and electronic conduction (MIEC), favorable microstructure and good chemical/thermal/mechanical stability along with significant catalytic activity.[15−17] Brownmillerite-type compounds that exhibit MIEC property can be considered as potential candidates in these classes of materials. Brownmillerite with a general formula of $A_2B_2O_5$ has alternate layers of BO_6 octaherda and BO_4 tetrahedra, creating inherent oxygen vacancies ordered in the tetrahedral layer.[18,19] The ordered oxygen vacancy in these materials can be distributed randomly by either high-temperature treatments or appropriate doping.[20−22] Such random distribution or disorder facilitates isotropic ionic conduction pathways, which is favorable for bulk diffusion properties, thereby increasing ionic conduction.[23] Also, doping with elements displaying good redox properties will enhance the catalytic properties in such systems.

In this context, we have developed a quasi-disordered Ce-doped brownmillerite, $Ba_2InCeO_{5+\delta}$, which shows comparable ORR activity with many other non-platinum systems.[13] In the present study, we have selected the series of compounds with the formula $Ba_2In_{2-x}Ce_xO_{5+\delta}$, where Ce is progressively doped in the In site and the effect of this doping on the structural aspects (i.e., disorder, oxygen vacancy, etc.) and ORR activity are investigated. Parent $Ba_2In_2O_5$ is a widely studied brownmillerite with stable lattice structure and ions in stable oxidation states.[24,25] The oxygen vacancies of $Ba_2In_2O_5$ become disordered at higher temperature (>930 °C), leading to excellent high-temperature MIEC property, which can be achieved at lower temperatures by doping. We chose Ce as dopant not only to induce oxygen vacancy disorder in the structure, but also to exploit its redox properties due to which it can be envisaged to be more tolerant to local changes in the oxygen concentration and may help increase ORR activity.[26,27] It was indeed observed that with an increase in the Ce concentration, ORR activity increased; but, interestingly, when In was completely replaced by Ce, making it a perfect

Received: September 16, 2014
Accepted: January 20, 2015
Published: January 20, 2015

DOI: 10.1021/am5087837
ACS Appl. Mater. Interfaces 2015, 7, 3041−3049

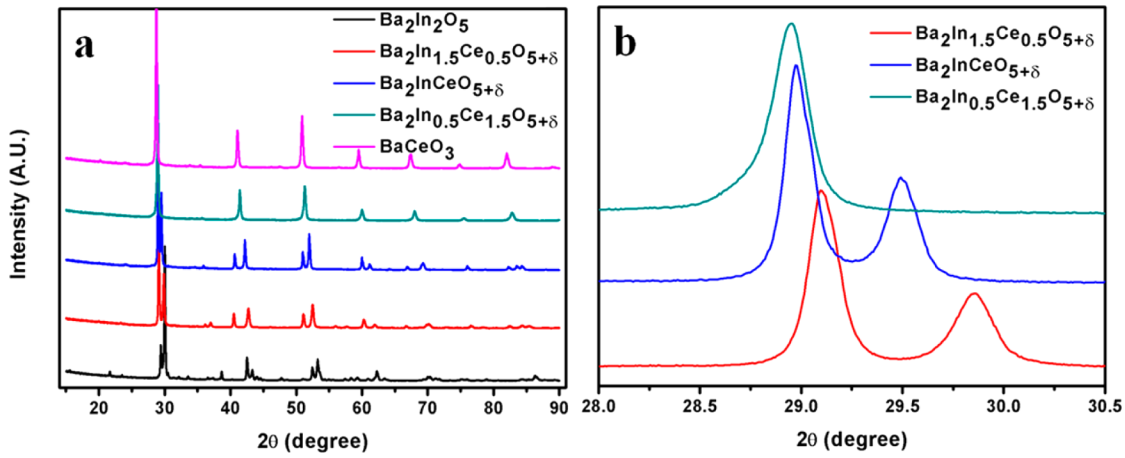

Figure 1. (a) PXRD pattern of $Ba_2In_{2-x}Ce_xO_{5+\delta}$ (x = 0, 0.5, 1, and 1.5) and $BaCeO_3$. (b) Enlarged portion of PXRD patterns of Ce-doped $Ba_2In_2O_5$.

perovskite structure, the ORR activity became poor. These observations support the fact that it is not only the dopant concentration but also the local structural characteristics pertaining to the oxygen vacancy disorder that affects the ORR activity.

2. EXPERIMENTAL SECTION

$Ba_2In_{2-x}Ce_xO_{5+\delta}$ was synthesized by solid state method. High purity $BaCO_3$ (99.98%, Sigma-Aldrich), In_2O_3 (99.99%, Sigma-Aldrich), and $Ce(CH_3CO_2)_3$ (99.9%, Sigma-Aldrich) were used as the starting materials. Stoichiometric amount of the starting materials were weighed and ball milled at 300 rpm for 3 h in Fristsch Pulverisette 6 Planetary Mill for homogeneous mixing. The samples were then calcined at 900 °C for 12 h. Subsequently, they were ground in a mortar and again calcined at 1200 °C for 8 h at a slow heating rate. $BaCeO_3$ was synthesized by combustion method using citric acid (99.5%, Merck) as fuel. An appropriate amount of $Ba(NO_3)_2$ (99.999%, Aldrich) and $(NH_4)_2Ce(NO_3)_6$ (99%, Merck) was added to citric acid solution and the pH of the solution was maintained at 7. The solution was heated at 80 °C to obtain a gel which was later calcined at 400 °C to remove the organic and volatile components. The powder was ground thoroughly and calcined at 900 °C for 8 h to obtain $BaCeO_3$. The phase purity of $Ba_2In_{2-x}Ce_xO_{5+\delta}$ series of compounds was determined by powder X-ray diffraction (PXRD) in PANalytical X'Pert Pro dual goniometer diffractometer with Ni filtered Cu Kα at 40 kV and 30 mA and X'celerator solid state detector with a step size of 0.008 and time per step 45.72 s. The diffraction pattern was obtained at room temperature in Bragg–Brentano geometry. Lattice parameters of the samples were calculated by Rietveld refinement method on the PXRD pattern using GSAS-EXPGUI program.[28] Raman spectra were recorded using Horiba JY LabRAM HR 800 which has a Czerny–Turner type spectrograph with 800 mm focal length and achromatic flat field monochromator along with mirror-based reflective optics and charge-couple device (CCD) detector. The scanned wavelength region was 50–1000 cm^{-1}, using He–Ne (632.8 nm, 20 mW) laser. The surface areas of the samples were determined by N_2 adsorption at the temperature of liquid nitrogen using the Autosorb iQ Quantachrome system. The samples were degassed at 300 °C under vacuum for 6 h prior to the analysis to remove the adsorbed moisture on the catalyst surface. The specific surface area was calculated using the BET model at relative pressure of P/P_0 = 0.05–0.3.

The electrochemical properties of the catalyst were measured by cyclic voltammetric (CV) and rotating disk electrode (RDE) analyses using a Biologic electrochemical workstation (SP-300) in a conventional three-electrode test cell with Hg/HgO and platinum foil as the reference and counter electrodes, respectively, under room temperature. For preparing the working electrode for CV and RDE measurements, we first polished glassy carbon (GC) electrode using 0.3 μm alumina and then the electrode was cleaned using deionized water. The catalyst for RDE was prepared by ball-milling (300 rpm for 90 min) a mixture of 100 mg of $Ba_2In_{2-x}Ce_xO_{5+\delta}$ with 25 mg of Vulcon XC-72 carbon. A slurry of catalyst was made by sonicating (BRANSON 1510) 5 mg of the sample-carbon composite in 1 mL 3:2 ethanol–water mixture for 1 h. A 10 μL aliquot of the catalyst slurry was drop-coated on the electrode surface. Subsequently, 2 μL of 0.01 wt % Nafion diluted with ethanol was applied on the whole surface of the electrode to yield a uniform thin film. This electrode was then dried in air and was used as the working electrode for all electrochemical studies. An aqueous solution of 0.1 M KOH (Aldrich, $\geq$ 85%) was used as the electrolyte for normal CV and RDE studies. Kinetics of oxygen reduction reactions of the catalyst were studied by using RDE, in 0.1 M KOH using a three-electrode cell assembly at a scan rate of 5 mV/s at 400, 900, 1200, 1600, 2000, and 2500 rpm at room temperature.

3. RESULTS AND DISCUSSION

$Ba_2In_{2-x}Ce_xO_{5+\delta}$ series of compounds with x = 0, 0.5, 1, and 1.5 was synthesized by solid state reaction while $BaCeO_3$ was synthesized by combustion method using citric acid. The phase purity of $Ba_2In_{2-x}Ce_xO_{5+\delta}$ was analyzed by PXRD. Figure 1a shows the comparison of PXRD patterns of the synthesized compounds.

The XRD pattern of $Ba_2In_2O_5$ matches with the orthorhombic alpha dibarium diindium oxide (JCPDS file No. 01-074-2662), while that of Ce-doped $Ba_2In_{1.5}Ce_{0.5}O_{5+\delta}$ matches with the tetragonal hydrated $Ba_2In_2O_5$ (JCPDS file No. 01-089-9079) with a very small fraction of CeO_2 as impurity. The other two Ce-doped compounds also crystallize in tetragonal system as explained later, with trace amounts of $BaCO_3$ impurity in $Ba_2InCeO_{5+\delta}$. XRD pattern of $BaCeO_3$ matches with already reported structure (JCPDS file No. 01-070-1429) with small amount of impurities of $BaCO_3$ and CeO_2. In the outset, it can be observed that with increase in the Ce concentration in $Ba_2In_2O_5$, the 2θ difference in the tetragonal splitting decreases, as shown in Figure 1b, indicating a gradual merger of a and c parameters. In $Ba_2In_{0.5}Ce_{1.5}O_{5+\delta}$, the splitting is not discernible in the broad peak indicating a highly disordered structure with random distribution of O atoms. Also, a shift toward the lower angle with increase in Ce concentration suggests an increase in the lattice parameters. The PXRD pattern with indexing is shown in Figures S1–S5 in Supporting Information

Structural parameters of the compounds are determined using Rietveld refinement of the XRD patterns using GSAS-

DOI: 10.1021/am5087837
ACS Appl. Mater. Interfaces 2015, 7, 3041–3049

Table 1. Structure Parameters Obtained from the Rietveld Refinement of $Ba_2In_{2-x}Ce_xO_{5+\delta}$ and $BaCeO_3$

		$Ba_2In_2O_5$[a]	$Ba_2In_{1.5}Ce_{0.5}O_{5+\delta}$[b]	$BaIn_{0.5}Ce_{0.5}O_{2.5+\delta}$[c]	$BaIn_{0.25}Ce_{0.75}O_{2.5+\delta}$[d]	$BaCeO_3$[e]
χ^2		3.154	1.967	3.202	3.402	4.365
wRp (%)		7.03	5.49	6.6	6.2	8.17
Rp (%)		4.79	3.9	4.51	4.37	5.64
space group		*Ima*2	*P*4/*mmm*	*P*4/*mmm*	*P*4/*mmm*	Pbnm
a (Å)		16.7777(2)	4.2466(0)	4.2902(0)	4.3448(0)	6.2229(5)
b (Å)		6.1013(1)	4.2466(0)	4.2902(0)	4.3448(0)	6.2173(6)
c (Å)		5.9731(1)	8.9298(1)	4.4434(0)	4.3682(1)	8.7859(6)
O 1	*x*	0.9910	0.5	0	0	0.071
	y	0.2832	0.5	0	0	0.487
	z	0.2491	0.244	0.5313	0.5167	0.25
occupancy		1	0.8242	0.4733	0.4949	1
O 2	*x*	0.1424	0	0	0	−0.274
	y	0.0639	0.5	0.5	0.5	0.278
	z	0.0540	0.5	−0.0464	0.0296	0.041
occupancy		1	0.9831	0.4238	0.4523	1
O 3	*x*	0.25	0.3558			
	y	0.9180	0			
	z	0.6398	0			
occupancy		1	0.5037			
$BaCO_3$ (wt %)				4.338		1.986
CeO_2 (wt %)						2.553

[a]$Ba_2In_2O_5$: Ba(0.1103,0.0133,0.5116), In1(0,0,0.0075), In2(0.25, 0.9420, 0.0268); [b]$Ba_2In_{1.5}Ce_{0.5}O_{5+\delta}$: Ba(0,0,0.2778), In1(0.5,0.5,0.5), In2-(0.5,0.5,0), Ce(0.5,0.5,0.5); [c]$BaIn_{0.5}Ce_{0.5}O_{2.5+\delta}$: Ba(0.5,0.5,0.5), In(0,0,0), Ce(0,0,0); [d]$BaIn_{0.25}Ce_{0.75}O_{2.5+\delta}$: Ba(0.5,0.5,0.5), In(0,0,0),Ce(0,0,0); [e]BaCeO3: Ba(0.001,0.023,0.25),Ce(0,0.5,0)

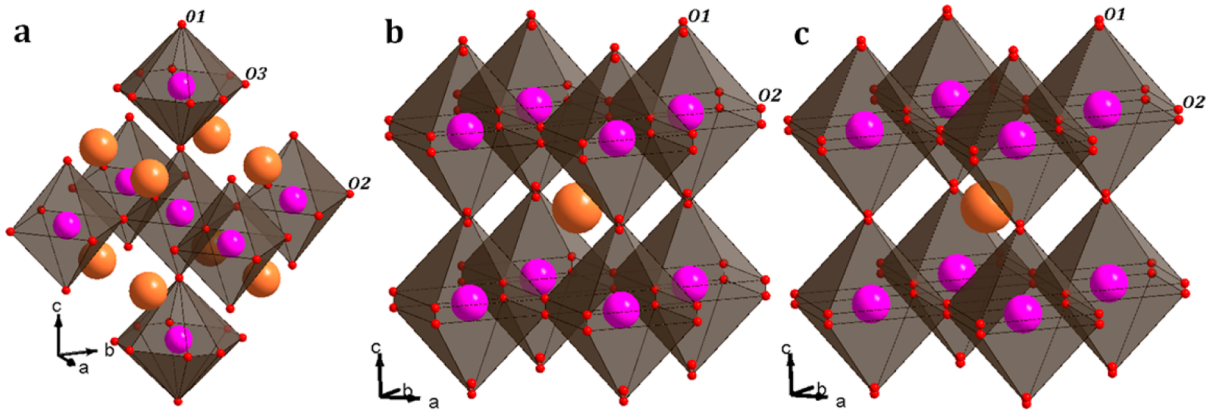

Figure 2. Polyhedral representation of the disordered structure obtained after the refinement for (a) $Ba_2In_{1.5}Ce_{0.5}O_{5+\delta}$, (b) $Ba_2InCeO_{5+\delta}$, and (c) $Ba_2In_{0.5}Ce_{1.5}O_{5+\delta}$.

EXPGUI. The detailed results of Rietveld refinement of $Ba_2In_{2-x}Ce_xO_{5+\delta}$ (x = 0, 0.5, 1, and 1.5) and $BaCeO_3$ are given in Table 1. The Rietveld refinement plots of the samples are shown in Figures S6−S10 in Supporting Information.

Rietveld refinement of $Ba_2In_2O_5$ was carried out using the structural parameter of alpha dibarium diindium oxide reported by Fischer et al.[29] Refinement of the XRD pattern with these parameters proceeded smoothly. The compound has a brownmillerite structure with alternative layers of In−O octahedra and tetrahedra. However, attempts to refine the structure of Ce-doped $Ba_2In_{1.5}Ce_{0.5}O_{5+\delta}$ with the orthorhombic structural parameters of the parent alpha $Ba_2In_2O_5$ were not fruitful. So, we proceeded with the cell parameters of the hydrated $Ba_2In_2O_5$; the refinement proceeded smoothly, and the XRD pattern fitted to tetragonal *P*4/*mmm* space group.[30] During the refinement, all the Ce atoms were manually assigned to the octahedral site because ionic size considerations prevent it from assuming tetrahedral geometry. In the case of $Ba_2InCeO_{5+\delta}$ and $Ba_2In_{0.5}Ce_{1.5}O_{5+\delta}$,with an increase in the Ce concentration, our attempt to refine the pattern with structural parameters of the hydrated one also was not successful. Hence, a new unit cell was arrived at with $c' \sim c/2$ of the hydrated $Ba_2In_2O_5$, and atomic coordinates were modified accordingly.[13] Rietveld refinement with these parameters proceeded smoothly. $BaCeO_3$ structural parameters could be refined on the basis of those reported by Jacobson et al.[31] $BaCeO_3$ being a perfect perovskite is expected to show an ideal cubic structure, but it deviates from the expected structure with *c* axis doubling due to octahedral tilting. It can be seen that the effective occupancy of O1 atom, which is along the *c* direction, increases gradually. This can be attributed to the fact that as Ce dopant concentration increases, the brownmillerite structure transforms to perovskite-like structure, leading to a disorder in the axial oxygen site. Finally, when it reaches a perfect perovskite structure, this disorder in oxygen site is absent. Similarly, the oxygen occupancy of the equatorial oxygen atom (O2)

DOI: 10.1021/am5087837
ACS Appl. Mater. Interfaces 2015, 7, 3041−3049

increases from $Ba_2InCeO_{5+\delta}$ to $Ba_2In_{0.5}Ce_{1.5}O_{5+\delta}$. The polyhedral representations of $Ba_2In_{1.5}Ce_{0.5}O_{5+\delta}$, $Ba_2InCeO_{5+\delta}$, and $Ba_2In_{0.5}Ce_{1.5}O_{5+\delta}$ are shown in Figure 2. The disorder in the O positions is easily seen from the figure, and a detailed discussion on this is given later.

The pseudocubic cell parameters of the samples were calculated and are plotted in Figure 3 (calculation details given in Supporting Information). It can be observed that with increase in Ce concentration, the *a* and *c* cell length values move close to each other, eventually shifting toward an ideal cubic structure. The gradual increase in the value of *a* and *b* axes can be ascribed to the larger crystal radius of Ce (1.15 and 1.01 Å for +3 and +4 oxidation state in octahedral coordination) than that of In (0.76 and 0.96 Å for octahedra and tetrahedral coordination).[32] But along the *c* direction, the lattice constant shoots up initially on 25% Ce substitution in In site and then decreases slowly. This may be because, in the case of $Ba_2In_{1.5}Ce_{0.5}O_{5+\delta}$, the brownmillerite structure with octahedral and tetrahedral layers is retained, and because the bigger Ce atom replaces the In in the octahedral site, it leads to an overall increase in the Ce/In−O bond distances. But with further increase in Ce concentration, the brownmillerite structure collapses, and disorder in O1 and O2 atoms along *c* aixs is observed (Figure 2). The distortion, as evident from distance between two equivalent O atoms along the *c* axis, decreases with further increase in the Ce concentration, resulting in gradual decrease in the lattice parameter along the *c* direction. Similarly, the gradual increase in the pseudocubic cell volume with increase in the Ce doping is due to larger crystal radius of Ce when compared with In (Figure 3). Interestingly, the extent of variation is very small in the substituted samples, indicating that other factors such as distortions and oxygen vacancies play a crucial role.

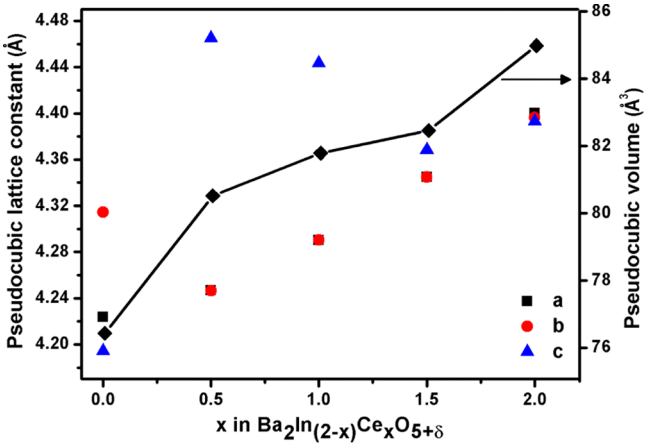

Figure 3. Pseudocubic cell parameters and pseudocubic cell volume of $Ba_2In_{2-x}Ce_xO_{5+\delta}$ as a function of substitution of *x*; for $BaCeO_3$, $x = 2$.

Table 2 shows the bond angles along the *c* direction (In/Ce−O1−In/Ce) and *ab* plane (In/Ce−O2−In/Ce) for Ce-doped $Ba_2In_2O_5$ systems. It can be noticed that the bond angle, In/Ce−O2−In/Ce initially decreases to 169° and then increases to 173.17° with increase in Ce concentration while the angle, In/Ce−O1−In/Ce along *c* direction remains same. The change in angle along *ab* plane can be attributed to distortion to a larger extent for $Ba_2InCeO_{5+\delta}$ when compared to $Ba_2In_{0.5}Ce_{1.5}O_{5+\delta}$. The same can be correlated with the disorder in the O1 and O2 position as shown in Figure 2 and the decrease in the lattice parameter along the *c* direction. The distance between the two equivalent positions for O1 atom is 0.279 Å and that for O2 atom is 0.413 Å for $Ba_2InCeO_{5+\delta}$, whereas in $Ba_2In_{0.5}Ce_{1.5}O_{5+\delta}$, it is 0.147 Å for O1 and 0.259 Å for O2 site. Also from Figure 2, it can be observed that in $Ba_2In_{1.5}Ce_{0.5}O_{5+\delta}$ there is a disorder in the O3 oxygen site in the *ab* plane. The structure is similar to that of hydrated $Ba_2In_2O_5$, in which the same disorder in O3 site is observed leading to an anisotropic two-dimensional layered structure with alternate layers of tetrahedra and octahedra.

The octahedral distortion, Δd for the Ce-doped systems was calculated to better understand this effect.[33] Δd was calculated according to the following equation

$$\Delta d = (1/6) \sum_{n=1,6} [(d_n - d)/d]^2$$

where *d* is the mean In/Ce−O bond distance, and d_n is the individual In/Ce−O bond distance of the compound. Table 3 shows the bond distance of the In/Ce−O and Δd calculated for the corresponding systems.

Table 3. In/Ce−O distance and bond Δd for $Ba_2In_{1.5}Ce_{0.5}O_{5+\delta}$, $Ba_2InCeO_{5+\delta}$ and $Ba_2In_{0.5}Ce_{1.5}O_{5+\delta}$

	$Ba_2In_{1.5}Ce_{0.5}O_{5+\delta}$	$Ba_2InCeO_{5+\delta}$	$Ba_2In_{0.5}Ce_{1.5}O_{5+\delta}$
In/Ce−O1	2.287	2.082	2.111
In/Ce−O1		2.361	2.257
In/Ce−O2	2.125	2.155	2.176
Δd	0.001244	0.001576	0.000377

It can be observed that the Δd value for $Ba_2In_{0.5}Ce_{1.5}O_{5+\delta}$ is lower than that for the other two systems. This suggests that a more symmetric environment is present around the In/Ce atom in $Ba_2In_{0.5}Ce_{1.5}O_{5+\delta}$.

In addition to the PXRD, Raman spectroscopy analysis was performed to get inputs on the structure. The Raman spectra of $Ba_2In_{2-x}Ce_xO_{5+\delta}$ and $BaCeO_3$ is shown in Figure 4.

Raman spectra of $Ba_2In_2O_5$ and $BaCeO_3$ match with already reported patterns in literature.[34,35] The bands in the low-frequency region, below 300 cm^{-1}, can be related to the vibrations mainly involving Ba^{2+} ions, which are the heaviest atoms in these compounds and hence are expected to vibrate at lower wavelengths. The appearance of peaks around 300−375 cm^{-1} is associated with the stretching vibration mode of CeO_6 octahedra. With an increase in the Ce concentration, intensities of these peaks increase, which is a clear indication of the enhanced presence of Ce in the octahedral site. In addition to

Table 2. Variation in the In/Ce−O−In/Ce Bond Angle along the *ab* Plane and *c* Direction

	$Ba_2In_{1.5}Ce_{0.5}O_{5+\delta}$	$Ba_2InCeO_{5+\delta}$	$Ba_2In_{0.5}Ce_{1.5}O_{5+\delta}$
In/Ce−O1−In/Ce (deg)[a]	180	180	180
In/Ce−O2−In/Ce (deg)[b]	180	169	173.17

[a]Along *c* direction. [b]In *ab* plane.

DOI: 10.1021/am5087837
ACS Appl. Mater. Interfaces 2015, 7, 3041−3049

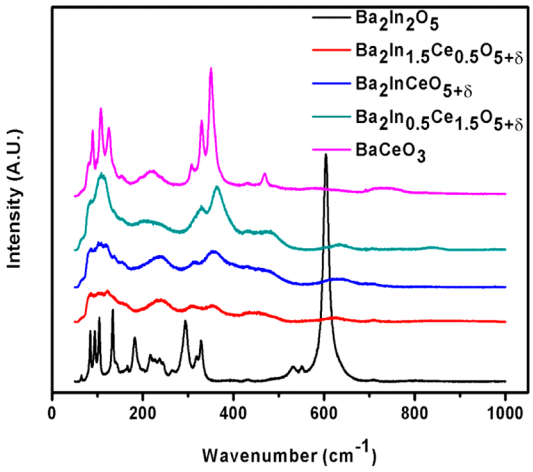

Figure 4. Raman spectra of $Ba_2In_{2-x}Ce_xO_{5+\delta}$ (x = 0, 0.5, 1, and 1.5) and $BaCeO_3$.

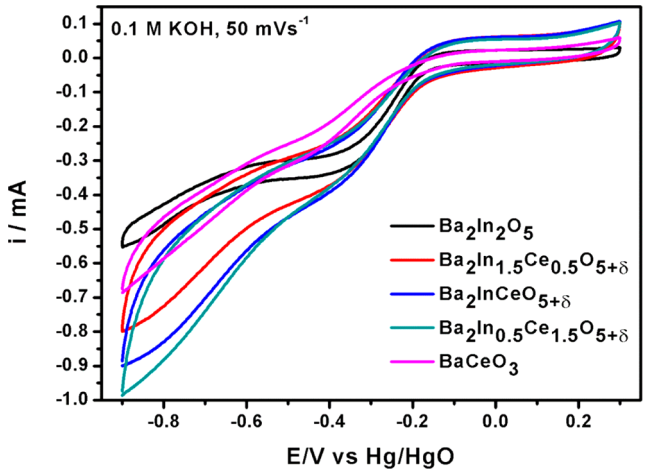

Figure 5. Cyclic voltammograms of $Ba_2In_{2-x}Ce_xO_{5+\delta}$ (x = 0, 0.5, 1, and 1.5) and $BaCeO_3$ in O_2 saturated 0.1 M KOH at a sweep rate of 50 mV s^{-1} with Hg/HgO as the reference electrode and Pt foil as the counter electrode.

the appearance of the peaks corresponding to CeO_6 octahedra, there is a drastic reduction in the intensity of the In−O bands that appear around 600 cm^{-1}, which is due to the disorder in the oxygen sublattice, as seen with other dopants.[24] The BET surface area of each sample was measured using N_2 adsorption study, and these values are reported in Table 4. The surface area obtained for the samples are very low, which can be attributed to their synthesis procedure.

Table 4. BET Surface Area of $Ba_2In_{2-x}Ce_xO_{5+\delta}$ (x = 0, 0.5, 1, and 1.5) and $BaCeO_3$ Calculated from N_2 Adsorption Study

sample	BET surface area (m^2/g)
$Ba_2In_2O_5$	5.393
$Ba_2In_{1.5}Ce_{0.5}O_{5+\delta}$	2.589
$Ba_2InCeO_{5+\delta}$	6.009
$Ba_2In_{0.5}Ce_{1.5}O_{5+\delta}$	3.781
$BaCeO_3$	6.218

Next, we carried out detailed electrochemical studies of these compounds for ORR activity in alkaline conditions using CV and RDE methods. For this, a slurry made by the mixture of the samples and Vulcon XC-72 carbon was coated on glassy carbon electrode. All the experiments were performed in 0.1 M KOH solution under room temperature. In our earlier study, any effect of carbon on the ORR activity of such oxides was ruled out.[13] Cyclic voltammograms of the samples under O_2 saturated solution at a sweep rate of 50 mV s^{-1} is shown in Figure 5.

From Figure 5, it is evident that with increase in the amount of Ce dopant in $Ba_2In_2O_5$, the current at an applied potential increases indicating an enhanced ORR activity. More cyclic voltammograms, generated during a detailed investigation of each sample in N_2 and O_2 saturated 0.1 M KOH solution, are given in the Supporting Information (Figures S11−S15), in which the increase in the current after O_2 purging indicates the ORR activity of the samples. Figure 6 shows the linear sweep voltammograms (LSV) of $Ba_2In_{2-x}Ce_xO_{5+\delta}$ (x = 0, 0.5, 1, and 1.5) and $BaCeO_3$ recorded at an electrode rotating speed of 2000 rpm in O_2 saturated 0.1 M KOH solution.

From Figure 6, it is clear that the onset potential of Ce-doped $Ba_2In_2O_5$ has a positive shift when compared to the two extreme compounds (i.e., $Ba_2In_2O_5$ and $BaCeO_3$). The onset

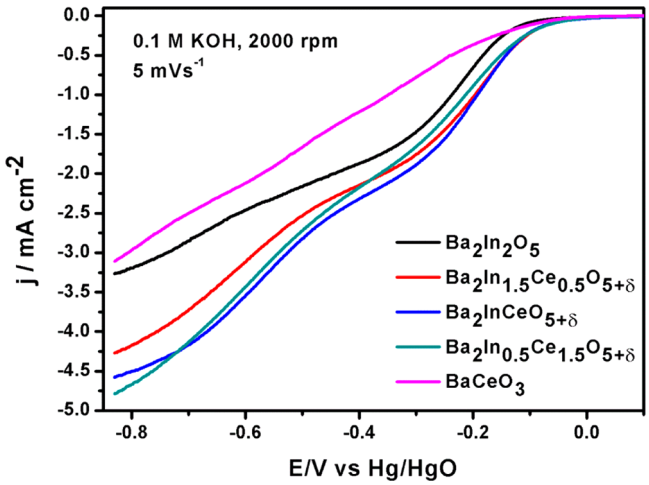

Figure 6. Hydrodynamic voltammograms obtained at an electrode rotating speed of 2000 rpm with a rotating disk electrode for the ORR on $Ba_2In_{2-x}Ce_xO_{5+\delta}$ (x = 0, 0.5, 1, and 1.5) and $BaCeO_3$. The experiments were performed in O_2-saturated 0.1 M KOH at a sweep rate of 5 mV s^{-1} using Hg/HgO as the reference electrode.

potential for all the Ce-doped samples is around −0.06 V Vs Hg/HgO, which is around 0.06 V more positive from the parent compounds. Apart from this, the geometrical limiting current density, which is a measure of the availability of active sites, increases with an increase in Ce concentration in $Ba_2In_2O_5$. However, it decreases again in the case of $BaCeO_3$ where there is no disorder in the axial and equatorial oxygen atoms. Figure 7 shows the LSVs of $Ba_2In_{2-x}Ce_xO_{5+\delta}$ (x = 0, 0.5, 1, and 1.5) and $BaCeO_3$ at various electrode rotation rates in O_2 saturated 0.1 M KOH solution. It is evident from Figure 7 that the limiting current density increases with the increase in the rate of rotation of the working electrode. This is a clear indication of the availability of the ORR active sites in the system. Also, a close analysis of the LSV profiles of the different systems reveals that at any constant rotation rate, the limiting current density increases with increase in the Ce concentration in $Ba_2In_2O_5$, and it eventually decreases in $BaCeO_3$ where Ce completely replaces In and enters into the perfect perovskite structure with no disorder in oxygen sites. It is important to

DOI: 10.1021/am5087837
ACS Appl. Mater. Interfaces 2015, 7, 3041−3049

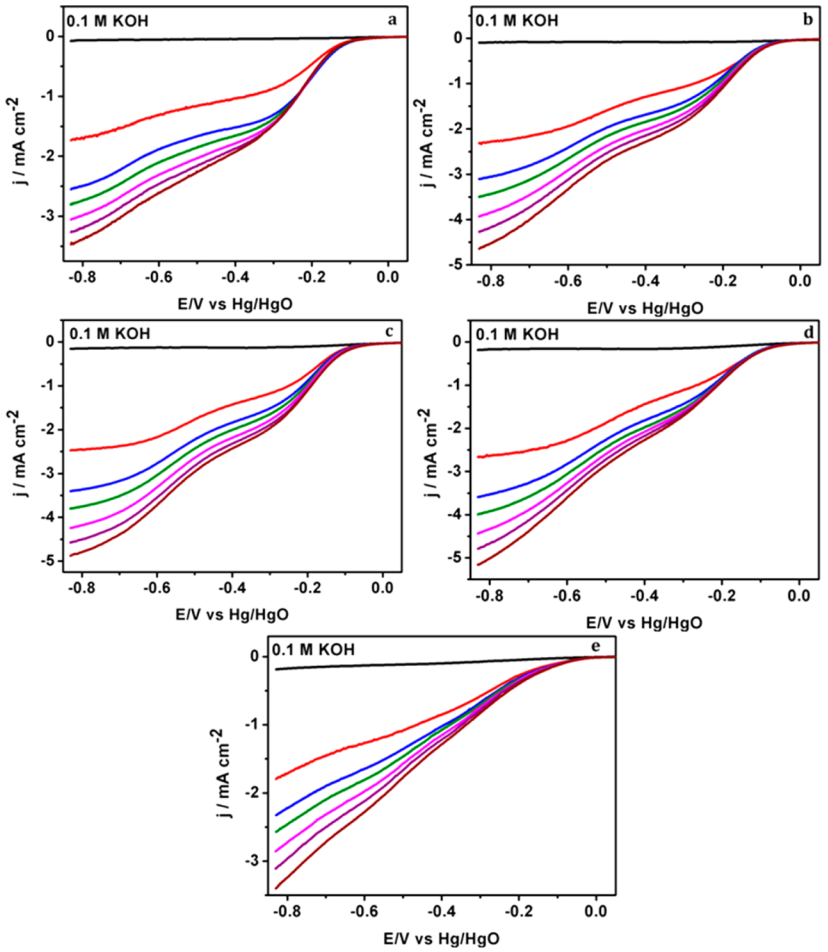

Figure 7. LSVs at different electrode rotation rates (black, blank; red, 400 rpm; blue, 900 rpm; green, 1200 rpm; pink, 1600 rpm; violet, 2000 rpm; and brown, 2500 rpm) for oxygen reduction reaction using (a) $Ba_2In_2O_5$, (b) $Ba_2In_{1.5}Ce_{0.5}O_{5+\delta}$, (c) $Ba_2InCeO_{5+\delta}$, (d) $Ba_2In_{0.5}Ce_{1.5}O_{5+\delta}$, and (e) $BaCeO_3$. The experiments were performed in O_2-saturated 0.1 M KOH at a sweep rate of 5 mV s^{-1} using Hg/HgO as the reference electrode.

note that as Ce concentration increases, ORR activity concomitantly increases, which can be expected because Ce is an excellent redox center. However, $BaCeO_3$, a stoichiometric perovskite without any oxygen vacancies and hence O_2 adsorption sites, exhibits very poor activity, and this proves that the mere presence of Ce is not enough for the material to be ORR active. Among the Ce-doped compounds, $Ba_2In_{1.5}Ce_{0.5}O_{5+\delta}$ with ordered tetrahedral and octahedral layers shows the least activity, whereas activity increases with an increase in disorder. This observation can be correlated with the fact that in $Ba_2In_{1.5}Ce_{0.5}O_{5+\delta}$, the layered structure will favor only anisotropic conduction, whereas disordered structures such as $Ba_2InCeO_{5+\delta}$ and $Ba_2In_{0.5}Ce_{1.5}O_{5+\delta}$ will have enhanced isotropic conduction. Also, we observe that among $Ba_2InCeO_{5+\delta}$ and $Ba_2In_{0.5}Ce_{1.5}O_{5+\delta}$, the latter has the least distorted octahedral environment around the In/Ce site. Such highly symmetric B site geometries are reported to play an active role in enhancing ionic conduction in doped $BaCeO_3$ compounds.[36] Hence, a synergistic influence of highly disordered yet symmetric Ce catalytic sites adjacent to oxygen vacancies can be deemed to be the important factor affecting the ORR activity of such oxides. This also suggests that it is not only the Ce which is enhancing the ORR activity, but the peculiar structural features like extent of disorder, B site symmetry, and so on also seem to have some effect.

The kinetic parameters such as electron transfer number, kinetic current density, and so on of samples is determined from the Koutecky–Levich (K–L) equation,

$$\frac{1}{j} = \frac{1}{nFkC_{O_2}} + \frac{1}{0.62nFC_{O_2}D_{O_2}^{2/3}\upsilon^{-1/6}\omega^{1/2}}$$

where j is the disk electrode current density, k is the reaction rate constant, n (mol^{-1}) is the number of electrons exchanged per O_2 molecule, F is the Faraday constant (96 500 C mol^{-1}), A is the electrode geometric area (0.196 cm^2), C_{O_2} is the bulk oxygen concentration (1.2×10^{-6} mol L^{-1}), D_{O_2} is the diffusion coefficient of molecular oxygen in 0.1 mol L^{-1} KOH solution (1.9×10^{-5} cm^2 s^{-1}), ν is the kinematic viscosity of the electrolyte (0.01 cm^2 s^{-1}) and ω is the electrode rotation speed in radians per second ($= 2\pi f = 2\pi$ rpm/60). A plot of the inverse of current (i^{-1}) as a function of the inverse of the square root of the rotation rate ($\omega^{-1/2}$), which is known as K–L plot, is a useful method to analyze the ORR kinetic parameters of an electro catalyst.[37] A comparison of the K–L plot of the various samples at −0.49 V is shown in Figure 8.

A clear change in the slope for $Ba_2In_{2-x}Ce_xO_{5+\delta}$ (x = 0.5, 1, and 1.5) from that of $Ba_2In_2O_5$ and $BaCeO_3$ is visible in Figure 8. This suggests that the ORR mechanism which can be either two-electron or four-electron mechanism are different for the two sets. With the information from the K–L plots, the number

DOI: 10.1021/am5087837
ACS Appl. Mater. Interfaces 2015, 7, 3041−3049

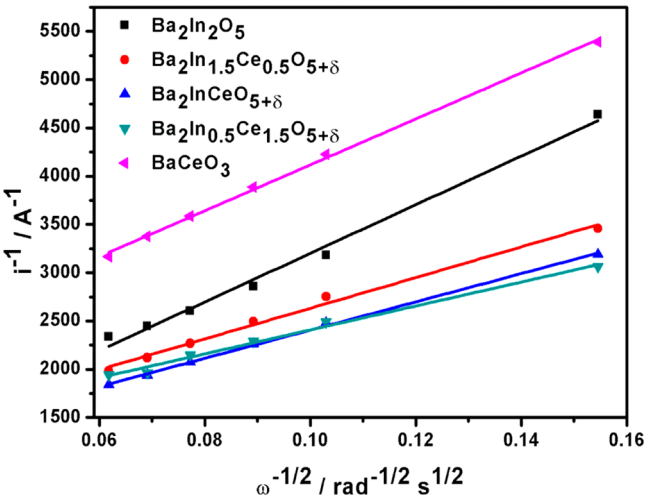

Figure 8. K–L plot of ORR on $Ba_2In_{2-x}Ce_xO_{5+\delta}$ (x = 0, 0.5, 1,and 1.5) and $BaCeO_3$ at a constant potential of −0.49 V in O_2 saturated 0.1 M KOH at a sweep rate of 5 mV s^{-1} using Hg/HgO as the reference electrode.

of electrons involved in the ORR mechanism is calculated. Figure 9 demonstrates the dependence of the applied potential on the electron transfer number in these samples.

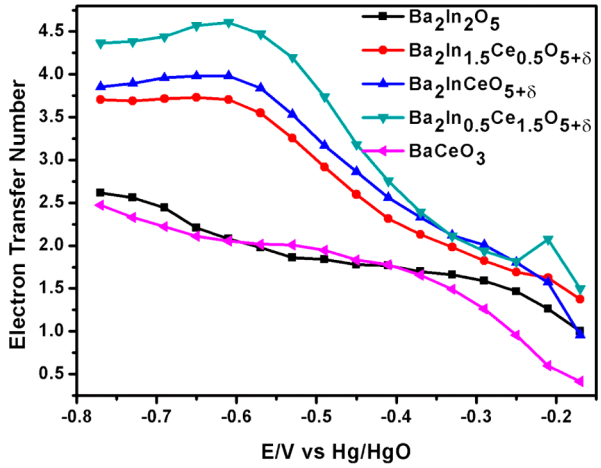

Figure 9. Dependence of the electron transfer number of $Ba_2In_{2-x}Ce_xO_{5+\delta}$ (x = 0, 0.5, 1, and 1.5) and $BaCeO_3$ on various applied potential in O_2 saturated 0.1 M KOH at a sweep rate of 5 mV s^{-1} using Hg/HgO as the reference electrode.

It is evident from Figure 9 that for $Ba_2In_2O_5$ and $BaCeO_3$, the number of electrons involved in the ORR is around 2 throughout the applied potential range, indicating that the reduction of oxygen occurs through peroxide intermediate. But in the other three samples, the electron transfer number for ORR is found to be ∼2 at lower negative potential and ∼4 at higher negative potential. In the intermediate region, the electron transfer number is found to be ∼3. The electron transfer number of 3 may be due to a parallel pathway involving both two- and four-electron mechanism.[38] This indicates that the applied potential has a significant role in deciding the kinetics of ORR reaction. The observed value of ∼4.5 at higher potentials in case of $Ba_2In_{0.5}Ce_{1.5}O_{5+\delta}$, which is above the theoretical value of 4, is due to parasitic current generated as a consequence of side reactions and chain reactions. The structural features mentioned above can be understood to play an important role in deciding the reaction pathway. Here also, the end members show different behavior to the doped compounds, and the number of electrons involved in the reaction increases with increase in the Ce dopant concentration. All the Ce doped $Ba_2In_2O_5$ with disorder in the O site shows appreciable ORR property with onset potential better than other oxide systems reported (Table S1, Supporting Information). We have also compared the activity with that of 40 wt % Pt/C standard catalyst, and found that the onset potential of the $Ba_2In_{2-x}Ce_xO_{5+\delta}$ oxides is only 0.05–0.1 V less than that of Pt/C. (Figure S16 in Supporting Information). This activity can also be further increased by fine-tuning the particle size and by improving the conductivity which will present a highly cost-effective electrode compared to the prohibitive Pt.

4. CONCLUSION

In summary, $Ba_2In_2O_5$ brownmillerites progressively Ce-doped in In site are tested for oxygen reduction activity in alkaline conditions. An interesting structural correlation emerged with respect to activity and disorder. The end members $Ba_2In_2O_5$ brownmillerite and $BaCeO_3$ perovskite are found to have poor activity for ORR. $Ba_2In_2O_5$ has an anisotropic structure in which In occupies alternate layers of tetrahedral and octahedral consequently giving rise to oxygen vacancies ordered in the tetrahedral layer. On the contrary, $BaCeO_3$ is a stoichiometric perovskite without any oxygen vacancies or disorder but with full occupancy of Ce in B site. Apparently, these features separately do not lead to good activity, but when combined, they affect the oxygen disorder, B site symmetry, and so on advantageously to present enhanced ORR activity in the doped compounds. On Ce(IV) doping in In(III) sites, oxygen vacancies are envisaged to be reduced but with enhanced disorder. The disorder occurs when the ordered layer structure collapses into 3D octahedral network as in the case of perovskites; now the structure has random oxygen vacancies in all three directions. Such disordered structures with isotropic conduction pathways are known to be better oxide ion conductors. Another parameter of interest is B site symmetry which measures the degree of distortion from an ideal octahedron, vis-à-vis bond lengths and bond angles. It is known that least distorted or most symmetric B sites enhance O_2 adsorption and oxide conduction. We observe an increase in B site symmetry as well, on increasing Ce dopant concentration. Hence, overall disorder and B site symmetry is enhanced by Ce doping leading to the ideal structure type, which presents catalytically active sites in the vicinity of adsorption sites, namely, oxygen vacancies. Such a confluence of all structural parameters is found in the 75% Ce-doped compound, which exhibits maximum limiting current comparable to standard catalysts with large concentrations of Pt. Moreover, these structural parameters also are found to have an impact on the reaction pathway through the number of electrons (four or two) involved in ORR which decides whether the reaction proceeds through the peroxide intermediate (two electrons). In the Ce-doped compounds, we observe a four-electron transfer at higher potential, indicating direct reduction of oxygen to hydroxide, which is more efficient and desirable.

DOI: 10.1021/am5087837
ACS Appl. Mater. Interfaces 2015, 7, 3041–3049

■ ASSOCIATED CONTENT

Supporting Information

Rietveld refinement plot, calculation of pseudocubic cell parameter cyclic voltammogram of all the samples, and linear sweep voltammogram of $Ba_2In_{2-x}Ce_xO_{5+\delta}$. This material is available free of charge via the Internet at http://pubs.acs.org.

■ AUTHOR INFORMATION

Corresponding Authors

* E-mail: nr.devi@ncl.res.in.
* E-mail: k.sreekumar@ncl.res.in.

Author Contributions

The manuscript was written through contributions of all authors. All authors have given approval to the final version of the manuscript.

Notes

The authors declare no competing financial interest.

■ ACKNOWLEDGMENTS

C.P.J. thanks CSIR, India, for financial support. Authors thank Richa Bobade for helping in Raman analysis.

■ REFERENCES

(1) Gasteiger, H. A.; Kocha, S. S.; Sompalli, B.; Wagner, F. T. Activity Benchmarks and Requirements for Pt, Pt-Alloy, and Non-Pt Oxygen Reduction Catalysts for PEMFCs. *Appl. Catal., B* **2005**, *56*, 9−35.

(2) Wang, B. Recent Development of Non-Platinum Catalysts for Oxygen Reduction Reaction. *J. Power Sources* **2005**, *152*, 1−15.

(3) Stephens, I. E. L.; Bondarenko, A. S.; Gronbjerg, U.; Rossmeisl, J.; Chorkendorff, I. Understanding the Electrocatalysis of Oxygen Reduction on Platinum and its Alloys. *Energy Environ. Sci.* **2012**, *5*, 6744−6762.

(4) Bashyam, R.; Zelenay, P. A Class of Non-Precious Metal Composite Catalysts for Fuel Cells. *Nature* **2006**, *443*, 63−66.

(5) Morozan, A.; Jousselme, B.; Palacin, S. Low-Platinum and Platinum-Free Catalysts for the Oxygen Reduction Reaction at Fuel Cell Cathodes. *Energy Environ. Sci.* **2011**, *4*, 1238−1254.

(6) Zhang, L.; Xia, Z. Mechanisms of Oxygen Reduction Reaction on Nitrogen-Doped Graphene for Fuel Cells. *J. Phys. Chem. C* **2011**, *115*, 11170−11176.

(7) Gong, K.; Du, F.; Xia, Z.; Durstock, M.; Dai, L. Nitrogen-Doped Carbon Nanotube Arrays with High Electrocatalytic Activity for Oxygen Reduction. *Science* **2009**, *323*, 760−764.

(8) Koslowski, U. I.; Abs-Wurmbach, I.; Fiechter, S.; Bogdanoff, P. Nature of the Catalytic Centers of Porphyrin-Based Electrocatalysts for the ORR: A Correlation of Kinetic Current Density with the Site Density of Fe−N_4 Centers. *J. Phys. Chem. C* **2008**, *112*, 15356−15366.

(9) Maruyama, J.; Okamura, J.; Miyazaki, K.; Uchimoto, Y.; Abe, I. Hemoglobin Pyropolymer Used as a Precursor of a Noble-Metal-Free Fuel Cell Cathode Catalyst. *J. Phys. Chem. C* **2008**, *112*, 2784−2790.

(10) Sunarso, J.; Torriero, A. A. J.; Zhou, W.; Howlett, P. C.; Forsyth, M. Oxygen Reduction Reaction Activity of La-Based Perovskite Oxides in Alkaline Medium: A Thin-Film Rotating Ring-Disk Electrode Study. *J. Phys. Chem. C* **2012**, *116*, 5827−5834.

(11) Suntivich, J.; Gasteiger, H. A.; Yabuuchi, N.; Nakanishi, H.; Goodenough, J. B.; Shao-Horn, Y. Design Principles for Oxygen-Reduction Activity on Perovskite Oxide Catalysts for Fuel Cells and Metal−Air Batteries. *Nat. Chem.* **2011**, *3*, 546−550.

(12) Grimaud, A.; May, K. J.; Carlton, C. E.; Lee, Y.-L.; Risch, M.; Hong, W. T.; Zhou, J.; Shao-Horn, Y. Double Perovskites as a Family of Highly Active Catalysts for Oxygen Evolution in Alkaline Solution. *Nat. Commun.* **2013**, *4*, 2439.

(13) Jijil, C. P.; Unni, S. M.; Sreekumar, K.; Devi, R. N. Disordered Brownmillerite $Ba_2InCeO_{5+\delta}$ with Enhanced Oxygen Reduction Activity. *Chem. Mater.* **2012**, *24*, 2823−2828.

(14) Saito, M.; Saito, Y.; Konishi, T.; Kawai, H.; Kuwano, J.; Shiroishi, H.; Uchimoto, Y. Electrocatalytic O_2 Reduction Properties of Pyrochlore-Type Oxides for Alkaline DAFCs. *ECS Trans.* **2008**, *16*, 891−900.

(15) Jiang, Y.; Wang, S.; Zhang, Y.; Yan, J.; Li, W. Kinetic Study of the Formation of Oxygen Vacancy on Lanthanum Manganite Electrodes. *J. Electrochem. Soc.* **1998**, *145*, 373−378.

(16) Liu, Y.; Tan, X.; Li, K. Mixed Conducting Ceramics for Catalytic Membrane Processing. *Catal. Rev.: Sci. Eng.* **2006**, *48*, 145−198.

(17) Zhou, W.; Sunarso, J.; Chen, Z.-G.; Ge, L.; Motuzas, J.; Zou, J.; Wang, G.; Julbe, A.; Zhu, Z. Novel B-Site Ordered Double Perovskite $Ba_2Bi_{0.1}Sc_{0.2}Co_{1.7}O_{6-x}$ for Highly Efficient Oxygen Reduction Reaction. *Energy Environ. Sci.* **2011**, *4*, 872−875.

(18) Antipov, E. V.; Abakumov, A. M.; Istomin, S. Y. Target-Aimed Synthesis of Anion-Deficient Perovskites. *Inorg. Chem.* **2008**, *47*, 8543−8552.

(19) Speakman, S. A.; Richardson, J. W.; Mitchell, B. J.; Misture, S. T. In-situ Diffraction Study Of $Ba_2In_2O_5$. *Solid State Ionics* **2002**, *149*, 247−259.

(20) Adler, S. B.; Reimer, J. A.; Baltisberger, J.; Werner, U. Chemical Structure and Oxygen Dynamics in $Ba_2In_2O_5$. *J. Am. Chem. Soc.* **1994**, *116*, 675−681.

(21) Yamamura, H.; Yamada, Y.; Mori, T.; Atake, T. Order−Disorder Transition of Oxygen Vacancy in the Brownmillerite System. *Solid State Ionics* **1998**, *108*, 377−381.

(22) Goodenough, J. B.; Ruiz-Diaz, J. E.; Zhen, Y. S. Oxide-Ion Conduction in $Ba_2In_2O_5$ and $Ba_3In_2MO_8$ (M = Ce, Hf, or Zr). *Solid State Ionics* **1990**, *44*, 21−31.

(23) Steele, B. C. H. Oxygen Ion Conductors and their Technological Applications. *Mater. Sci. Eng., B* **1992**, *13*, 79−87.

(24) Shin, J. F.; Orera, A.; Apperley, D. C.; Slater, P. R. Oxyanion Doping Strategies to Enhance the Ionic Conductivity in $Ba_2In_2O_5$. *J. Mater. Chem.* **2011**, *21*, 874−879.

(25) Mohn, C. E.; Allan, N. L.; Freeman, C. L.; Ravindran, P.; Stolen, S. Collective Ionic Motion in Oxide Fast-Ion-Conductors. *Phys. Chem. Chem. Phys.* **2004**, *6*, 3052−3055.

(26) Aneggi, E.; Boaro, M.; Leitenburg, C. d.; Dolcetti, G.; Trovarelli, A. Insights into the Redox Properties of Ceria-Based Oxides and their Implications in Catalysis. *J. Alloy. Compd.* **2006**, *408−412*, 1096−1102.

(27) Malacrida, P.; Escudero-Escribano, M.; Verdaguer-Casadevall, A.; Stephens, I. E. L.; Chorkendorff, I. Enhanced Activity and Stability of Pt−La and Pt−Ce Alloys for Oxygen Electroreduction: The Elucidation of the Active Surface Phase. *J. Mater. Chem. A* **2014**, *2*, 4234−4243.

(28) Toby, B. H. EXPGUI, A Graphical User Interface for GSAS. *J. Appl. Crystallogr.* **2001**, *34*, 210−213.

(29) Fischer, W.; Reck, G.; Schober, T. Phase Transition of $Ba_2In_2O_5$ in Humid Air Studied by in Situ X-ray Powder Diffraction. *Mater. Sci. Forum* **2000**, *321*, 363−367.

(30) Fischer, W.; Reck, G.; Schober, T. Structural Transformation of the Oxygen and Proton Conductor $Ba_2In_2O_5$ in Humid Air: An in Situ X-ray Powder Diffraction Study. *Solid State Ionics* **1999**, *116*, 211−215.

(31) Jacobson, A. J.; Tofield, B. C.; Fender, B. E. F. The Structures of $BaCeO_3$, $BaPrO_3$, and $BaTbO_3$ by Neutron Diffraction: Lattice Parameter Relations and Ionic Radii in O-Perovskites. *Acta Crystallogr., Sect. B: Struct. Sci.* **1972**, *28*, 956−961.

(32) Shannon, R. Revised Effective Ionic Radii and Systematic Studies of Interatomic Distances in Halides and Chalcogenides. *Acta Crystallogr., Sect. A: Cryst. Phys., Diffr., Theor. Gen. Crystallogr.* **1976**, *32*, 751−767.

(33) Malavasi, L.; Kim, H.; Proffen, T. Local and Average Structures of the Proton Conducting Y-Doped Baceo3 from Neutron Diffraction and Neutron Pair Distribution Function Analysis. *J. Appl. Phys.* **2009**, *105*, 123519−1−123519−10.

(34) Karlsson, M.; Matic, A.; Knee, C. S.; Ahmed, I.; Eriksson, S. G.; Börjesson, L. Short-Range Structure of Proton-Conducting Perovskite $BaIn_xZr_{1-x}O_{3-x/2}$ (x = 0−0.75). *Chem. Mater.* **2008**, *20*, 3480−3486.

DOI: 10.1021/am5087837
ACS Appl. Mater. Interfaces 2015, 7, 3041−3049

(35) Scherban, T.; Villeneuve, R.; Abello, L.; Lucazeau, G. Raman Scattering Study of $BaCeO_3$ and $SrCeO_3$. *Solid State Commun.* **1992**, *84*, 341−344.
(36) Malavasi, L.; Ritter, C.; Chiodelli, G. Correlation between Thermal Properties, Electrical Conductivity, and Crystal Structure in the $BaCe_{0.80}Y_{0.20}O_{2.9}$ Proton Conductor. *Chem. Mater.* **2008**, *20*, 2343−2351.
(37) Wang, S.; Yu, D.; Dai, L.; Chang, D. W.; Baek, J.-B. Polyelectrolyte-Functionalized Graphene as Metal-Free Electrocatalysts for Oxygen Reduction. *ACS Nano* **2011**, *5*, 6202−6209.
(38) Wang, S.; Yu, D.; Dai, L. Polyelectrolyte Functionalized Carbon Nanotubes as Efficient Metal-free Electrocatalysts for Oxygen Reduction. *J. Am. Chem. Soc.* **2011**, *133*, 5182−5185.

DOI: 10.1021/am5087837
ACS Appl. Mater. Interfaces 2015, 7, 3041−3049